energies

MDPI

Article

Mechanical Deterioration Mechanism of Inter-Turn Insulation in Dry-Type Air-Core Reactors

Minhu Xu [1], Chang Liu [1], Xuedong Wang [1], Zhenchuan Wang [1], Fuyu Cao [2] and Hongyan Nie [2,*]

[1] Heilongjiang Electric Power Research Institute, Harbin 150080, China; 18645051218@163.com (M.X.); 18008262339@163.com (C.L.); 15636084121@163.com (X.W.); 15776802683@163.com (Z.W.)
[2] Key Laboratory of Engineering Dielectrics and Its Application, Harbin University of Science and Technology, Harbin 150080, China; 18943748206@163.com
* Correspondence: niehongyan@hrbust.edu.cn

Abstract

Polyester (PET) inter-turn insulation of dry-type air-core reactors endures long-term compressive stress induced by internal pre-tightening force and temperature fluctuation during service, which easily induces microcrack propagation and accelerated insulation breakdown. Existing studies mainly focus on thermal, electrothermal and hygrothermal aging of PET films, while few investigations reveal the mechanical degradation laws under various compressive stresses sustained during reactor operation. To fill this research gap, this paper develops a continuous compressive loading test platform matched with an exponentially damped oscillating voltage (EDOV) test system. Thermal- and damp-heat-pretreated PET specimens are prepared via accelerated aging methods to simulate actual operating environments. Combined with impulse withstand tests and dielectric loss characterization, the micro-damage evolution and insulation performance decay rules under multi-gradient compressive stress are analyzed. The results indicate that under sustained compressive stress, progressive microcrack growth and property decay are observed, with a more pronounced degradation for specimens subjected to prior thermal or damp-heat aging treatment. The findings can provide quantitative support for reactor on-site insulation assessment, condition monitoring and maintenance strategy formulation.

Keywords: dry-type air-core reactor; mechanical aging; PET; insulation degradation analysis; property characterization

Check for updates

Academic Editor: Constantinos S. Psomopoulos

Received: 29 September 2026
Revised: 22 October 2026
Accepted: 29 October 2026
Published: 1 November 2026

Copyright: © 2026 by the authors. Licensee MDPI, Basel, Switzerland. This article is an open access article distributed under the terms and conditions of the Creative Commons Attribution (CC BY) license.

1. Introduction

With the development of power systems toward ultra-high-voltage transmission, large capacity, and a high penetration of renewable energy sources [1,2], dry-type air-core reactors have been widely used in reactive-power compensation, overvoltage suppression, and short-circuit current limitation because of their absence of magnetic saturation, good linearity, and low maintenance requirements. They are therefore essential equipment for secure and stable grid operation [3–5]. Field operation statistics indicate that an inter-turn insulation short circuit is the most frequent and most severe failure mode of dry-type air-core reactors. Once the insulation deteriorates, inter-turn short circuits, local overheating, and even fire or explosion may occur, leading to equipment damage, large-scale power outages, substantial economic losses, and serious safety risks [6–9].

During long-term operation, the inter-turn insulation of reactors is subjected to coupled electrical, thermal, mechanical, and damp-heat stresses. Among these factors, mechanical

compressive stress is a key driver of insulation degradation. Winding pre-tightening pressure, electromagnetic force during operation, and thermal expansion/contraction caused by temperature variation can all generate sustained compressive stress inside the insulation. In cold regions in particular, large temperature excursions intensify thermal-expansion mismatch and stress concentration, thereby inducing the initiation and propagation of microcracks as well as interfacial debonding, which markedly accelerates insulation deterioration [10]. Compressive stress not only directly degrades the mechanical properties of insulating materials, but also acts together with thermal stress, damp-heat stress, and switching overvoltage [11], thereby substantially reducing the dielectric strength and switching-impulse withstand capability of the insulation. It is consequently a major cause of early failure of inter-turn insulation [12,13].

A large number of existing studies have investigated the thermal, electrothermal and hygrothermal aging characteristics of polyester films. These works reveal the chemical deterioration mechanism dominated by molecular chain scission and oxidation, and establish corresponding temperature-based life prediction models [14]. However, most mechanical property tests of PET adopt short-time tensile or transient compression loading, failing to simulate the long-term compressive stress formed by pre-tightening force and temperature gradient inside dry-type air-core reactors. Few publications focus on the microcrack evolution and breakdown life decay of PET inter-turn insulation under various compressive stresses during reactor operation. Different from the conventional research framework of electrothermal aging, this paper carries out multi-gradient compression accelerated aging tests and conducts systematic microcrack characterization and withstand performance statistical analysis, which fills the research gap regarding mechanical compression deterioration of PET insulation for reactors.

Numerical and frequency-response studies have further shown that inter-turn short circuits and local temperature rise can rapidly change reactor winding characteristics and intensify insulation degradation [15]. Existing studies have mainly focused on thermal aging, electrical aging, and overvoltage impulse characteristics of inter-turn insulation, revealing such phenomena as the reduction in mechanical properties by thermal aging and cumulative breakdown induced by switching overvoltage [16–20]. Polyester film is the primary material used in inter-turn insulation. However, the deterioration mechanism and quantitative behavior of polyester film under individual mechanical stresses remain insufficiently investigated, and the relationship between microstructural damage and macroscopic property decay has not been adequately established. Using the number of switching-overvoltage withstand operations as a macroscopic lifetime indicator, and dielectric loss as a microscopic diagnostic parameter, is consistent with the practical operating conditions of reactors. It is therefore necessary to investigate the deterioration mechanism of polyester film under sustained mechanical stress.

2. Preparation of Aged Specimens and Experimental Platform

2.1. Mechanical Stress Aging Device and Stress Levels

A simple device capable of continuously applying mechanical stress was designed and fabricated. The main components include mechanical jacks, spring sets, smooth metal disks, and a channel-steel frame.

The structure of the device is shown in Figure 1.

By adjusting the lift of the jack, the spring set is compressed to a specified length. The elastic potential energy stored in the spring set is converted into a continuous mechanical load, and the magnitude of the load is monitored in real time by a pressure sensor calibrated against standard weights before each test. The smooth metal disks have a diameter of 25 mm; periodic re-verification of the spring compression was performed to compensate for

load drift caused by spring and PET relaxation, confirming that the load remained within ±5% of the nominal value throughout the 600 h aging. Once the preset compressive stress is achieved, we stop adjusting the jack. The mechanical stress is transmitted to the surface of the insulating specimen through the smooth metal disks, thereby simulating the contact stress sustained by reactor inter-turn insulation in service.

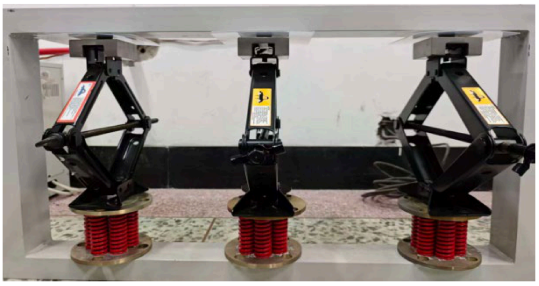


Figure 1. Photograph of the mechanical stress aging device.

Before testing, a large-range pressure sensor was used to determine the spring displacement corresponding to the target load. The pressure required for the experiment was obtained from

$$F = P \cdot S = M \cdot g \quad (1)$$

where P is the pressure required for aging, S is the area of the metal disk, g is taken as 9.8 m/s^2, and M is the load provided by the jack expressed in kilograms.

During long-term service of dry-type air-core reactors, the winding pre-tightening force and axial temperature gradient continuously generate compressive stress on inter-turn insulation. A thermal-structure coupling finite element simulation from Xu et al. reveals that the average equivalent compressive stress of the intact epoxy encapsulation matrix under rated operation is approximately 9.5 MPa [21]. The reactor temperature rises gradually from bottom to top, and the difference in thermal expansion results in lower stress at the low-temperature bottom and higher stress at the high-temperature upper region.

To fully cover the actual load conditions of on-site reactors, three equal-gradient compressive stresses of 4 MPa, 8 MPa and 12 MPa are adopted for aging tests in this work. The medium benchmark stress is selected as 8 MPa, which is close to the typical steady-state operating stress of 9.5 MPa provided in the reference. A stress of 4 MPa simulates the low stress state under light load and low temperature with favorable heat dissipation, while 12 MPa represents the high stress concentration condition caused by equipment overload and local hot spots. The equal 4 MPa interval can quantitatively characterize the acceleration effect of compressive stress on the withstand degradation of PET insulation.

Accordingly, normal loads of 200, 400, and 600 kg supplied by the jack are required to apply pressures of 4, 8, and 12 MPa, respectively.

The compressive load is exerted by a jack, and the pressure sensor is fully calibrated in advance. The jack's lifting stroke is slowly adjusted until the sensor reads the target stress, and the corresponding compression length of the spring is recorded. With the overall installation position unchanged, the spring is adjusted to this calibrated length for load calibration before every test. After calibration, six layers of PET specimens are neatly stacked. Since all specimens possess identical material properties, every layer can bear uniform compressive pressure. Aligned metal disks are arranged on the top and bottom of the specimen stack. Subsequently, the jack is lifted to make the spring assembly reach the pre-calibrated compression displacement to apply stable compressive stress. All PET sheet specimens adopted in the tests have dimensions of 150 mm× 150 mm× 0.05 mm.

2.2. EDOV Test Device

To reproduce the switching overvoltage generated during practical reactor switching operations, an EDOV generator was built with reference to IEC 60076-6:2007, Clause 12.8.11 (switching-impulse test) and Annex E (turn-to-turn overvoltage test for dry-type reactors). The test device and its schematic diagram are shown in Figure 2.

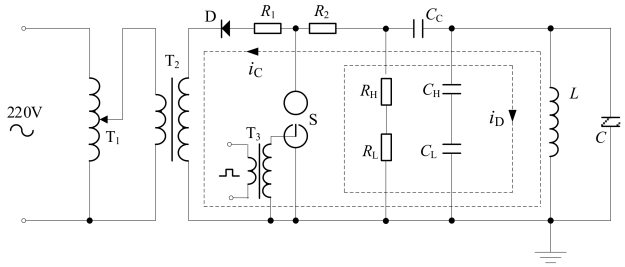


Figure 2. Schematic of the EDOV test device.

During the charging stage, which corresponds to the negative half-cycle of the power supply, the high-voltage silicon stack D conducts and the sphere-gap switch S remains open. The test transformer T_2, the high-voltage silicon stack D, the protective resistor R_1, the damping resistor R_2, the main capacitor C_C, and the inductor L form a closed charging circuit, and the main capacitor is charged by the power-frequency source to the preset voltage. During the discharge stage, corresponding to the positive half-cycle, the high-voltage silicon stack D is blocked and the sphere-gap switch S is triggered into conduction. The main capacitor C_C discharges through the damping resistor R_2 into the inductor L, causing periodic conversion between electric-field energy and magnetic-field energy. When R_2 is lower than the critical damping value, an EDOV is produced across the inductor L. Throughout this process, the energy periodically transfers between C_C and L and is gradually dissipated in R_2. With an appropriate R_2 value, the required EDOV waveform can be obtained across the inductor.

A digital oscilloscope was used to record and display the voltage waveform during testing. The displayed waveform is shown in Figure 3.

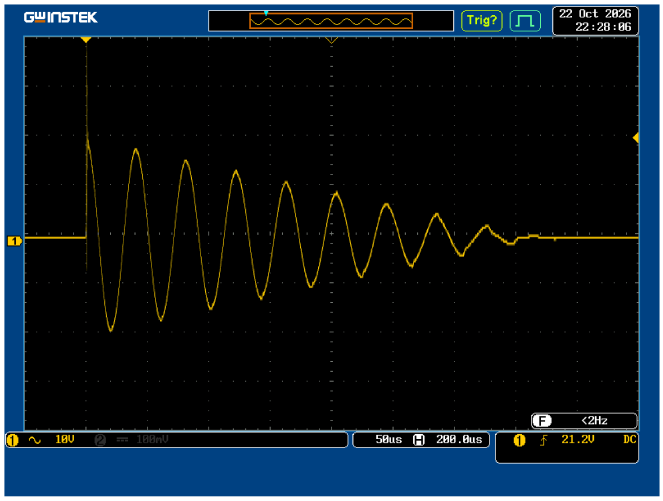


Figure 3. Waveform of EDOV at the test voltage of 21 kV captured by the oscilloscope.

The device generated the required EDOV waveform, with a peak value of 180 kV, which represents the maximum output capability of the generator; the actual test voltage applied in this study is 21 kV. The main capacitance is $C_C = 3$ nF, the inductance is $L \approx 14$ mH

(corresponding to an oscillation frequency of about 24.6 kHz), and the damping resistance is $R_2 \approx 2$ kΩ; the protective resistance and the preset charging voltage were selected to produce the required 21 kV waveform. It can output 3000 standard waveforms per minute, which satisfies the specified test repetition rate and substantially reduces the experimental duration. Cylindrical electrodes with a diameter of 25 mm and a 3 mm chamfer were selected, and six layers of 0.05 mm PET film specimens were connected in parallel for simultaneous withstand-voltage testing. Enlarged specimen dimensions were adopted to increase the creepage distance and suppress surface discharge along the film edges.

3. Mechanical Stress Aging

3.1. Compressive Stress Aging and Accelerated Thermal Aging

To further investigate the influence of aging time on the mechanical and electrical deterioration of polyester film sheet specimens, five aging durations were designed, with 120 h defined as one mechanical aging cycle. This duration is selected to balance accelerated aging efficiency and measurable accumulation of microstructural damage under continuous compression. A subset of specimens was removed and sealed after each cycle. To examine the effect of compressive stress aging on the dielectric properties of specimens that had already experienced mechanical property degradation, two types of thermally aged specimens were further aged for 240 h under three stress levels. The dielectric properties and impulse-voltage withstand characteristics of all aged specimens were then investigated.

A large number of studies have shown that reactors inevitably suffer thermal stress aging during operation. However, the effect of thermal stress is mainly reflected in the decline of mechanical properties, whereas its influence on dielectric withstand performance is comparatively limited [22]. Considering the environmental factors encountered by reactors in service, single-factor thermal aging and damp-heat cyclic aging tests were performed on polyester film sheet specimens using accelerated aging methods. Specimens with degraded mechanical properties were thereby obtained and subsequently subjected to mechanical stress aging, with the aim of clarifying the overvoltage withstand behavior of specimens with different mechanical-property states after mechanical stress exposure.

Single polyester film specimens were used in the accelerated thermal aging test and stacked in six layers. To ensure uniform heating, the specimens were clamped onto a mesh tray. According to GB 10229-1988 and IEC 60289:1988 [23,24], the long-term operating temperature of the reactor is set to 80 °C. Substituting this temperature into the Class B insulation life formula (2) gives

$$\tau_B = 10^{\left(\frac{4808.121}{273+80} - 7.533\right)} = 1.224 \times 10^6 \text{ h} \approx 139 \text{ years} \tag{2}$$

The insulation life at 80 °C is approximately 139 years. Preliminary tests show that the electrode system becomes structurally unstable above 170 °C, so 160 °C is selected as the accelerated aging temperature.

$$\begin{cases} \tau_B = 10^{\left(\frac{4808.121}{273+160} - 7.533\right)} = 3725 \text{ h} \\ T = \frac{15 \times 365 \times 24}{1.224 \times 10^6} \times 3725 = 399.9 \approx 400 \text{ h} \end{cases} \tag{3}$$

Using the Class B insulation life model, 15 years of reactor operation at 80 °C is equivalent to about 400 h aging at 160 °C.

To simulate and accelerate the most severe environmental stresses encountered by reactors in service, a damp-heat cyclic aging experiment with clear engineering relevance was designed. Condensation caused by day-night temperature differences or start-stop operation, prolonged humid conditions in wet climates or rainy seasons, condensation of residual internal hot gas during abrupt temperature drops, and rainwater ingress due to

package damage can all wet the insulation layer and thereby directly or indirectly accelerate insulation deterioration. Accelerated damp-heat cyclic aging of polyester film specimens was implemented in a GDJW-100 alternating temperature-humidity test chamber. This chamber adopts closed-loop real-time automatic control to stably maintain preset temperature and humidity parameters throughout the aging cycle without manual adjustment. The procedure was as follows:

(1) High-temperature dry-heat stage: Specimens were placed in a constant-temperature oven and aged for 50 h in dry air at 160 °C.

(2) High-temperature high-humidity stage: Specimens were then transferred to a constant-temperature and constant-humidity chamber and aged for 24 h at 80 °C and 95% relative humidity. Preliminary tests and literature results indicate that the properties of polyester materials, such as elongation at break and dielectric strength, decrease very slowly in dry air at 80 °C. This means that, in the absence of humidity, chemical-structure changes caused by pure thermal aging at 80 °C may be regarded as secondary within the experimental duration. Therefore, the 80 °C/95% RH stage in this experiment is essentially a strengthened moisture absorption and hydrolysis condition. The role of 80 °C is to relax the polymer microstructure and provide channels and reaction activity for water molecules; it is not the primary aging stress source. The dominant driving force is the high humidity of 95% RH, while 80 °C accelerates this moisture-related aging process.

The high-temperature dry-heat and high-temperature high-humidity stages were performed consecutively. The two stages lasted 74 h in total and were defined as one complete damp-heat cyclic aging cycle. Four such cycles were interspersed within the 400 h thermal-aging schedule, so that the damp-heat group experienced periodic moisture-and-hydrolysis exposure superimposed on the thermal-aging baseline.

At the end of each aging cycle, 12 specimens were removed for frequency-domain dielectric spectroscopy. Subsequently, cumulative breakdown tests under overvoltage, namely EDOV, were conducted. To shorten the test duration and suppress the effect of air discharge at the electrodes, an EDOV with an amplitude of 21 kV was selected as the test voltage. The cumulative number of EDOV applications sustained by a specimen until breakdown was taken as the lifetime endpoint; after removing the maximum and minimum values, ten valid data points were retained.

3.2. Mechanical Property Testing

Mechanical properties are direct macroscopic indicators for evaluating the aging degree of insulating materials. In this study, uniaxial tensile tests were performed on dumbbell-shaped specimens according to GB/T 1040.3. Two key parameters were obtained: elongation at break (%), which is highly sensitive to aging and reflects material toughness; and tensile strength (MPa), which reflects the load-bearing capacity of the material.

Twelve specimens of each of the two thermally aged groups were removed at different aging cycles, cut into dumbbell-shaped specimens according to the standard, and tested for tensile strength and elongation at break using a universal testing machine. The maximum and minimum values were discarded, and the average of the remaining results was used. The obtained elongation at break and tensile strength are shown in Figure 4.

The variation in tensile strength and elongation at break of PET films under the two aging conditions shows that the mechanical properties of the specimens continuously deteriorate with aging time. Nevertheless, the magnitude, rate, and underlying mechanism of degradation differ markedly between single-factor thermal aging and damp-heat cyclic aging. During single-factor thermal aging, both tensile strength and elongation at break decrease slowly, and the overall mechanical performance remains relatively stable.

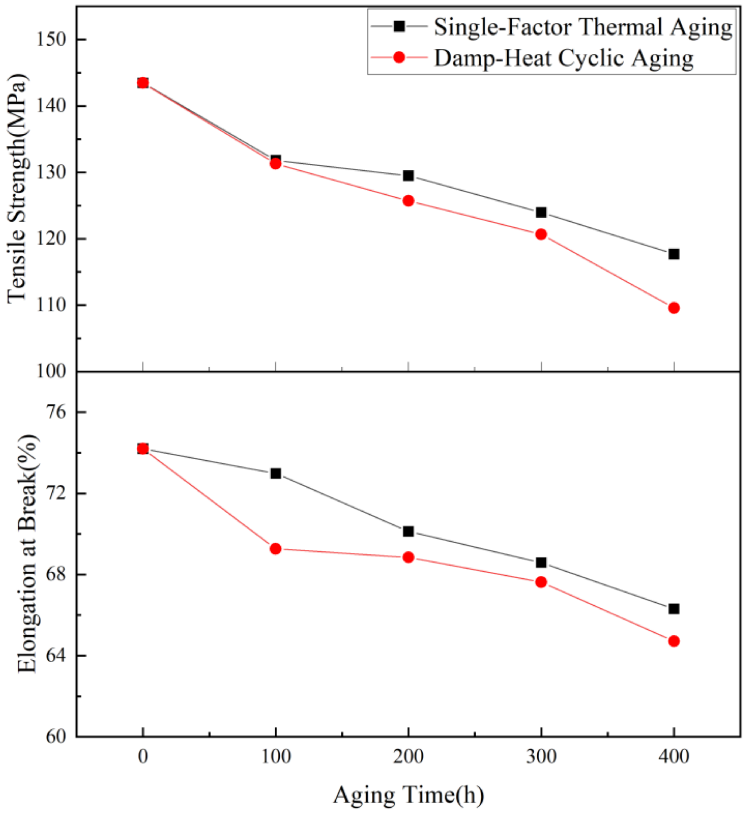


Figure 4. Mechanical properties of the two groups of aged specimens as a function of thermal aging time.

Two distinct stages can be distinguished in the evolution of mechanical properties. In the first 100 h, tensile strength remains nearly unchanged because it is borne mainly by the crystalline and oriented skeleton; oxidation and hydrolysis act initially on the amorphous region without disrupting the load-bearing network, and moisture primarily exerts a plasticizing effect rather than chain scission. Thereafter, accumulated oxidation and hydrolysis reach the crystal-amorphous interface, and the strength begins a gradual decline. Elongation at break shows a different sensitivity: it remains nearly unchanged in the first 100 h (entanglement intact, limited chain scission), then decreases approximately linearly, which is consistent with near-first-order hydrolytic chain scission and a progressive reduction in molecular weight that embrittles the material. The damp-heat group declines more steeply because hydrolysis directly scissions chains in the amorphous region.

For mechanically aged specimens subjected to different stress levels and aging durations, dumbbell-shaped specimens were cut from the aged region and tested for mechanical strength. The tensile strength and elongation at break are shown in Figure 5.

The results indicate that, regardless of the applied stress level, mechanical strength decreases with increasing aging time. The overall trend is characterized by a rapid initial decrease followed by a slower decline. Higher applied stress produces more pronounced mechanical deterioration.

To quantify the decay kinetics, the measured data in Figure 5 were fitted to $\sigma(t) = \sigma\infty + (\sigma_0 - \sigma\infty)\cdot\exp(-t/\tau)$. The fitted time constants and coefficients of determination are summarized in Table 1.

Table 1. Fitted decay time constants and coefficients of determination of PET film under different compressive stresses.

Applied Stress (MPa)	Elongation at Break τ (h)	Elongation at Break R^2	Tensile Strength τ (h)	Tensile Strength R^2
4	656	0.992	250	0.970
8	378.6	0.995	274.7	0.995
12	210	0.988	222.9	0.982

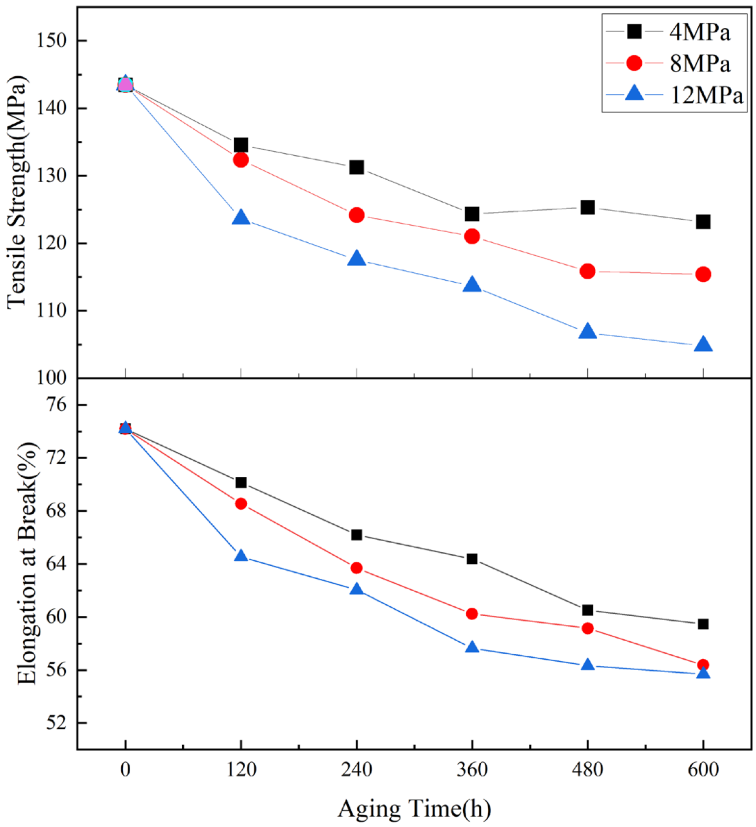


Figure 5. Mechanical properties of initially unaged specimens as a function of mechanical aging time.

The time constant τ of elongation at break decreases monotonically with applied stress, approximately halving for each 4 MPa increment, whereas τ of tensile strength shows no clear monotonic trend. This contrast indicates that compressive stress primarily accelerates the loss of ductility (elongation at break, reflecting chain scission in the amorphous region); the decay rate of tensile strength, borne mainly by the crystalline skeleton, is less stress-dependent, and the effect of stress on strength manifests mainly in the total degradation amplitude rather than in the decay rate.

4. Mechanical Deterioration Mechanism Under Different Aging Conditions

4.1. Overvoltage Withstand Count After Mechanical Stress Aging

Unpretreated polyester film specimens were aged at 4, 8, and 12 MPa, respectively, with 120 h defined as one aging cycle and five cycles applied at each stress level. After aging, the overvoltage withstand count was measured. Each group was tested 12 times; after removing the maximum and minimum values, the results shown in Figure 6 were obtained. Multi-cycle aging tests on unpretreated polyester film specimens under compressive stresses of 4, 8, and 12 MPa show that the overvoltage withstand count decreases continuously with increasing stress level and aging duration. Under low stress (4 MPa), the material

response is dominated by elastic and plastic deformation. The molecular chains gradually compact under sustained compression, and few internal defects are generated; therefore, the withstand count decreases slowly. When the stress increases to 8 and 12 MPa, microcracks and micropores are more likely to initiate in regions of internal stress concentration. As aging proceeds, these defects expand and interconnect, forming electric-field concentration sites and charge traps, reducing the partial-discharge inception voltage, and accelerating the formation of breakdown paths. For the same aging duration, higher stress corresponds to a lower withstand count, and degradation exhibits a clear acceleration feature under high stress.

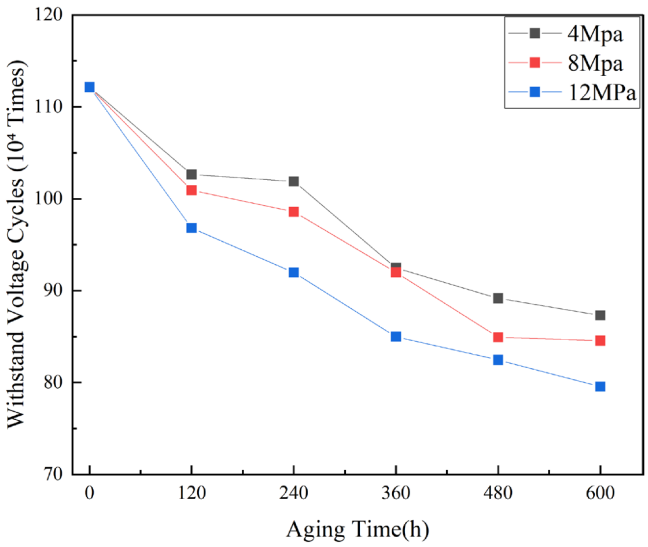


Figure 6. Withstand count versus aging time under different stresses.

The 95% confidence interval of the endurance life at each stress point is calculated based on the t-distribution for small samples. For each test condition, ten repeated specimens are measured. The confidence interval is expressed as:

$$CI = \bar{x} \pm t_{\alpha/2}(n-1)\frac{s}{\sqrt{n}} \quad (4)$$

where $\bar{x}$ is the sample mean, s is the sample standard deviation, $n = 10$ is the number of replicates, and $t_{\alpha/2}(n-1) = 2.2622$ corresponds to the two-tailed t-value at the 95% confidence level with 9 degrees of freedom.

To quantify the dispersion of withstand test data, the 95% t-distribution confidence intervals for each working condition are calculated and summarized in Table 2.

Table 2. 95% confidence intervals of withstand breakdown cycles of PET insulation under different compressive stresses and aging durations.

Aging Time/h	4 MPa CI	8 MPa CI	12 MPa CI
120	17,221.6	108,262.5	134,411.7
240	62,351.7	72,259.8	64,377.0
360	112,450.2	30,943.0	54,802.3
480	91,024.1	118,010.3	152,978.1
600	111,560.5	77,906.6	78,586.1

The confidence interval range generally expands with the rise in compressive stress, which reflects higher data dispersion under large mechanical loads. For a fixed stress level, data dispersion decreases first and then increases with aging time, reaching its minimum value during the medium aging stage of 240–360 h.

4.2. Withstand Count After Thermal and Mechanical Aging

To evaluate the degradation effect of thermal aging and damp-heat cyclic aging on the dielectric withstand performance of polyester film, the number of switching-impulse withstand operations was measured for specimens at aging stages of 0, 100, 200, 300, and 400 h, where each 100 h interval corresponds to one aging cycle. This test was used to reveal the evolution of insulation performance during aging.

The withstand-count data of specimens subjected to the two thermal aging conditions are shown in Figure 7.

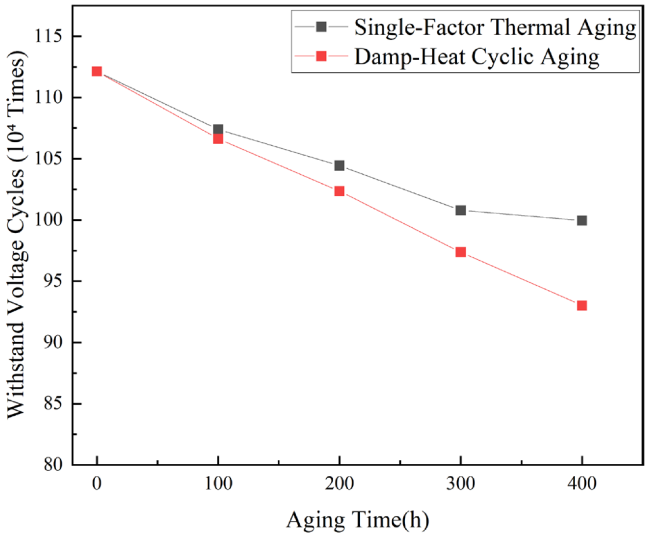


Figure 7. Overvoltage withstand count of the two groups of aged specimens as a function of aging time.

Under a 21 kV EDOV, the withstand counts of both specimen groups decrease with aging time. The degradation magnitude and rate of the damp-heat cyclically aged specimens are significantly higher than those of the single-factor thermally aged specimens.

The initial withstand count is 1.1215×10^6. After 400 h of single-factor thermal aging, the retention rate is 89.13%, showing a slow, approximately linear decline. After 400 h of damp-heat cyclic aging, the retention rate decreases to only 82.95%, exhibiting an accelerated behavior characterized by an initial slow decrease followed by a rapid decline. The overvoltage withstand counts of the single-factor thermally aged and damp-heat cyclically aged specimens after 240 h of aging under three different stress levels are compared in Figure 8.

The overvoltage withstand capability of the three specimen groups under 4, 8, and 12 MPa is shown in Figure 8.

After 240 h of mechanical compressive stress aging, the withstand counts of the unaged, single-factor thermally aged, and damp-heat cyclically aged specimens all decrease with increasing stress. At the same stress level, the order is unaged specimens > single-factor thermally aged specimens > damp-heat cyclically aged specimens, which is consistent with the mechanical-property degradation trend. The damp-heat cyclically aged specimens exhibit the most severe decrease in withstand count as the stress increases.

These results show that prior thermal or damp-heat aging changes the subsequent response to compressive stress. The differences in withstand count among the three specimen groups indicate that mechanical deterioration should be assessed in relation to the initial material condition. The sequential test design does not establish an independent additive law for these degradation processes.

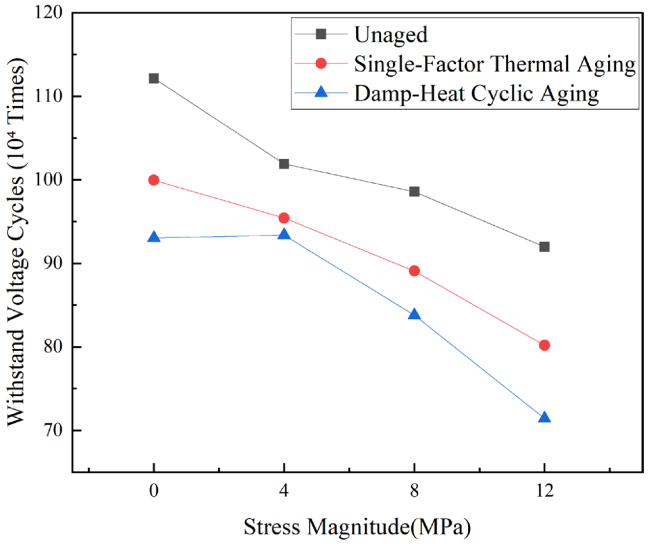


Figure 8. Effect of aging stress level on the overvoltage withstand count of three specimen groups.

4.3. Dielectric Loss After Mechanical Aging

The dielectric-loss variation in unpretreated specimens aged under 12 MPa compressive stress was first measured using an IDAX-300 system. The results are shown in Figure 9.

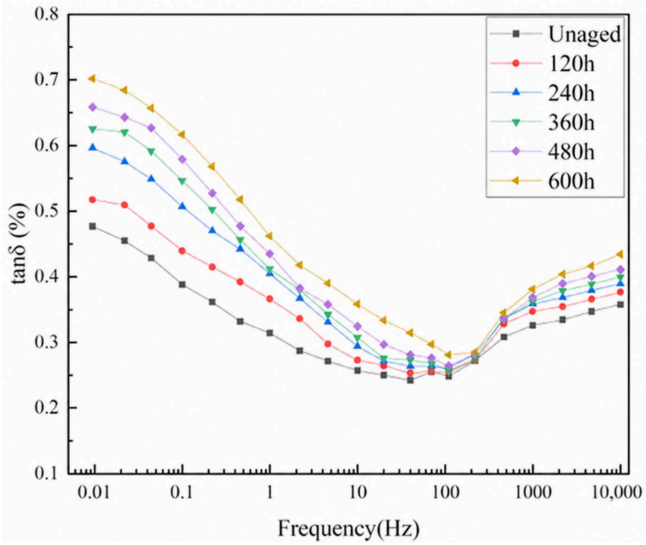


Figure 9. Dielectric-loss variation in PET with aging time under 12 MPa compressive stress aging.

After mechanical compressive stress exposure, the dielectric loss of polyester film increases significantly over the entire frequency range with aging time, and the low-frequency range (0.01–10 Hz) is the most sensitive. The loss increases rapidly in the early aging stage, rises slowly in the middle stage, and tends to stabilize in the later stage, indicating that the stress-induced structural damage and defect development gradually approach saturation. The applied stress not only promotes the formation of internal microcracks and strengthens interfacial polarization and space-charge effects, but also reduces insulation resistance and increases conductive loss.

The tan delta behavior near 100 Hz reflects two competing polarization mechanisms. The slow decrease from 0.01 to 100 Hz is attributed to interfacial and space-charge polarization, which are slow processes that gradually lag behind the alternating field as frequency rises. The subsequent increase above approximately 100 Hz is attributed to the onset of

the PET dipolar beta-relaxation, corresponding to local motion of amorphous-region chain segments, whose contribution grows at mid-to-high frequencies.

Dielectric loss was then measured for the two groups of mechanically degraded specimens after 240 h of exposure to different stress levels. The results are shown in Figure 10.

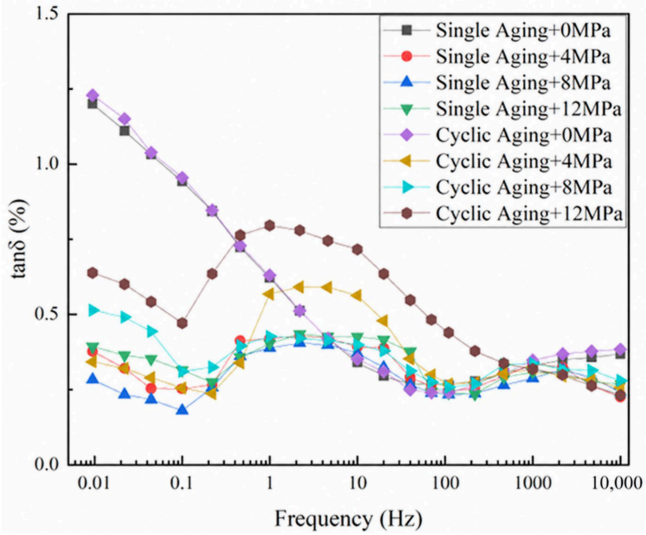


Figure 10. Dielectric loss of the two groups of thermally aged specimens after aging under different stress levels.

Comparison of the dielectric loss of the two types of 400 h thermally aged specimens after 240 h of aging under different stress levels shows that their loss curves exhibit broadly similar trends: the loss decreases markedly in the low-frequency region, while increasing over 0.1–100 Hz, with a raised peak in the mid-frequency region. A likely reason is that both 400 h thermal aging conditions generate numerous microcracks on the surface or inside the material. Mechanical stress can partially close these microcracks, reducing the air-gap volume and thereby markedly decreasing the interfacial-polarization loss in the low-frequency range. At the same time, mechanical stress reduces insulation resistance and thus increases conductive loss. This behavior differs from that of unaged specimens. Because unaged specimens have smooth surfaces and no obvious defects, externally applied stress tends to generate microcracks; meanwhile, mechanical stress aging reduces insulation resistance, causing loss to increase over the whole frequency range, with a larger increase at low frequencies.

This result also explains why damp-heat cyclically aged specimens subjected to 4 MPa aging may show a higher overvoltage withstand count than mechanically aged specimens. Under low stress, pre-existing microcracks may be compressed to smaller dimensions and few additional microcracks are generated, thereby reducing the overall partial-discharge intensity and the erosive effect of discharge on the insulation. The dielectric strength therefore shows a short-term increase. Under higher stress, however, a larger number of microcracks are generated, and the withstand count decreases sharply.

The frequency shift between stressed and unstressed specimens indicates a change in the dominant polarization mechanism. Under compression, newly generated microcracks and pores form large-scale interfaces that give strong MWS (Maxwell-Wagner-Sillars) polarization, whose characteristic response lies in the low-frequency range (0.01–10 Hz). In the uncompressed or thermally aged specimens, loss variation is dominated by molecular dipolar beta-relaxation, whose characteristic frequency lies near 100 Hz and above. Thus compressive stress shifts the dominant polarization toward lower frequencies by introducing large-scale interfacial defects.

The two degradation scenarios should be distinguished. For unpretreated specimens under compression (Figure 9), newly generated microcracks create additional interfacial area, strengthening low-frequency MWS polarization and increasing the loss. For pre-aged specimens (Figure 10), the pre-existing microcracks are partially closed by the applied stress, which reduces the interfacial-polarization loss at low frequencies; meanwhile, the stress-induced reduction in insulation resistance increases the conductive loss in the mid-frequency range. The apparent difference in frequency response therefore originates from whether microcracks are newly generated or compression-closed, which is consistent with the microscopic observations in Section 4.4.

4.4. Optical Observation of PET Microcracks

To illustrate the evolution of micro-defects in PET insulation during compressive stress aging, optical micrographs of specimens aged under 4 MPa, 8 MPa and 12 MPa for 120 h, 240 h, 360 h and 480 h are presented in Figure 11.

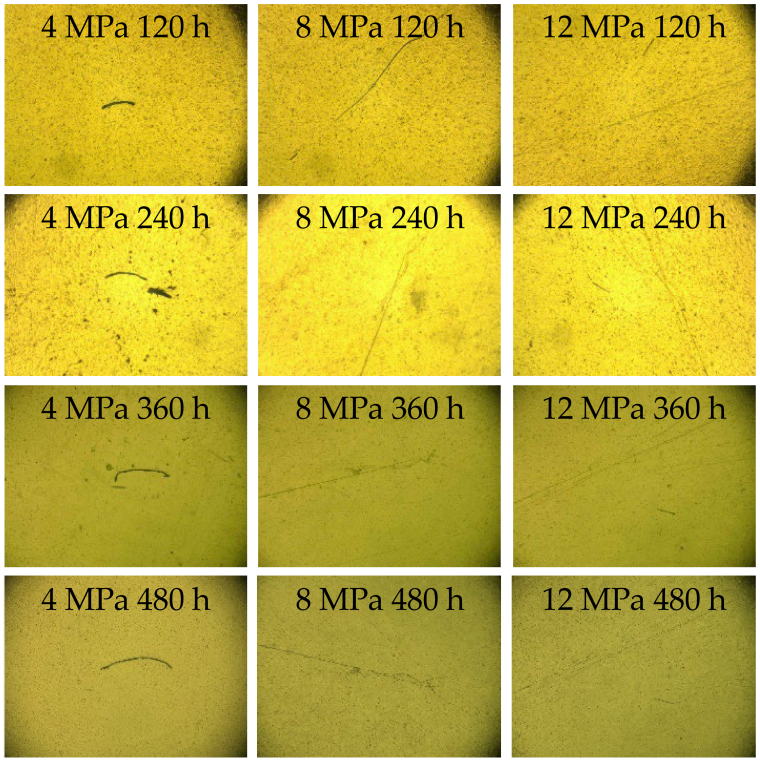


Figure 11. Optical microscope images of polyester film under various compressive stresses and aging durations.

The evolution process of microcrack initiation and propagation is analyzed by comparative observation.

The surface of unaged specimens is flat and smooth, without obvious micropores, microcracks or other defects. After compressive stress aging, microcracks emerge rapidly under all three stress levels. As aging time increases, the generated microcracks continuously extend and widen. After several aging periods, the growth rate of cracks decreases significantly, and the crack size tends to stabilize.

The compressive stress magnitude exerts a remarkable influence on microcrack development. For the same aging duration, higher compressive stress induces more microcracks and larger crack sizes on the specimen surface.

The above microscopic observations directly confirm that compressive stress is the primary factor triggering the generation and continuous propagation of microcracks in PET

insulation. Higher stress accelerates crack initiation and promotes defect accumulation. From a microscopic perspective, this explains the macroscopic experimental trend that the insulation withstand life declines markedly with rising compressive stress, and provides intuitive microscopic experimental evidence for the exponential decay of mechanical properties with aging time (fitted in Figure 5).

4.5. Mechanical Deterioration Mechanism

The deterioration of polyester film under mechanical compressive stress follows a complete evolutionary path of structural deformation, defect initiation, crack propagation, property decay, and breakdown failure. The core mechanism can be summarized as follows.

First, mechanical compressive stress directly drives deterioration. Sustained compressive stress causes compression, orientation, and rearrangement of polyester molecular chains. Under low stress, the material structure tends to become denser; under high stress, stress concentration occurs in internal weak regions, inducing molecular-chain scission, micropores, and microcrack initiation [25]. With increasing aging time, microcracks continue to propagate and interconnect, forming conductive paths and electric-field concentration sites. This reduces dielectric strength and the breakdown threshold, which is ultimately manifested as a pronounced decrease in the overvoltage withstand count.

Second, single-factor thermal aging relaxes polymer chains and reduces toughness, whereas damp-heat aging involves water molecule ingress and hydrolysis reactions, which significantly weaken intermolecular interactions and severely degrade mechanical properties. These aging processes reduce the material resistance to deformation and crack propagation, making structural damage more likely under mechanical stress. Thermal or damp-heat pretreatment therefore changes the initial mechanical state on which compressive stress acts. The greater deterioration of the damp-heat group is consistent with moisture-related weakening of PET [19]. The relative contributions of these processes depend on the aging history and cannot be separated quantitatively by the present sequential tests.

Third, microstructural evolution is directly coupled with macroscopic performance. Microstructural changes caused by mechanical stress determine the macroscopic electrical and mechanical properties. In initially unpretreated specimens, newly generated microcracks and interfacial defects are associated with increased low-frequency dielectric loss. In pre-aged specimens, compression-induced closure of existing cracks can instead reduce this contribution, as discussed in Section 4.3. Destruction of structural integrity reduces tensile strength and elongation at break and weakens the switching-overvoltage withstand capability. Dielectric-loss spectra should therefore be interpreted together with mechanical properties, microscopic observations and withstand count when relating macroscopic performance to microscopic damage.

In summary, mechanical compressive stress is a major contributor to inter-turn insulation deterioration, while thermal and damp-heat environments play significant accelerating roles. Microcrack initiation and propagation, together with molecular-chain structural evolution, constitute the core degradation mechanism. These processes ultimately reduce dielectric strength and lead to breakdown failure. The deterioration mechanism is illustrated in Figure 12. This study did not include a time-matched unloaded control under identical stacking, disk contact, and environmental conditions; the independent contribution of environmental exposure to the observed degradation cannot be fully excluded. A dedicated control study is planned as future work.

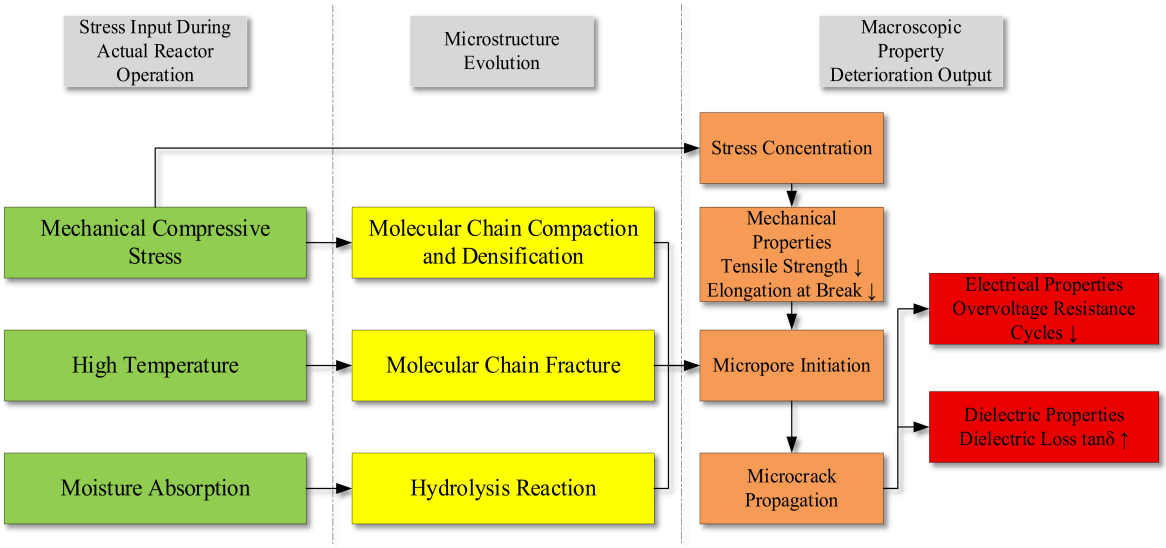


Figure 12. Mechanical deterioration mechanism.

4.6. Mitigation Measures and Assessment Under Operating Conditions

The observed dependence of microcracking and withstand count on compressive stress suggests that mitigation should focus on limiting local stress concentrations while retaining adequate winding restraint. During design and assembly, the clamping load should be distributed uniformly, and uneven supports, sharp contact edges and excessive local preload should be avoided. The restraint should also accommodate differential thermal expansion during changes in load and ambient temperature. Reducing preload alone is insufficient because the winding must retain mechanical stability under normal operation and fault forces.

Thermal and moisture control are complementary measures because the pre-aged specimens generally exhibited greater deterioration under subsequent compression. Maintaining ventilation passages and limiting local overheating can reduce thermal exposure and the associated expansion mismatch. Inspection and repair of damaged encapsulation, together with drainage and protection against condensation and water ingress, can limit moisture exposure. Where insulation materials or coatings are changed, their moisture resistance, thermal endurance and mechanical compatibility should be evaluated together [19]. Switching transients should also be considered in insulation coordination: mitigation measures should be selected according to the inter-turn voltage waveform and its distribution within the winding, rather than terminal voltage magnitude alone [11,13].

Comprehensive assessment should begin with the operating history, including load current, temperature rise and thermal cycling, ambient humidity and condensation, and switching events. These records help identify whether thermal aging, moisture exposure, mechanical loading or repetitive electrical stress is likely to dominate. Local mechanical stress should be estimated from the winding structure, assembly condition and validated thermomechanical analysis; the specimen test stresses should not be treated as universal service-stress thresholds. Visual inspection of encapsulation and supports, combined with temperature monitoring, can then locate regions requiring closer examination.

Electrical measurements should complement these observations. During an outage, suitably controlled oscillating-voltage partial-discharge measurements can help identify active insulation defects [26], while winding frequency-response measurements can provide complementary evidence of inter-turn short-circuit abnormalities [6]. Comparisons should use a commissioning baseline or a comparable sound unit under consistent test connections and environmental conditions. Where representative material samples are available from

maintenance or retired units, dielectric-loss spectra, tensile properties and microscopy can be used to relate electrical changes to embrittlement and cracking. These material tests and the cumulative EDOV breakdown test are laboratory assessments; the measured withstand count is not a direct measure of the remaining operating life of an installed reactor.

The indicators should be interpreted jointly because different mechanisms can produce competing responses. Section 4.3 shows that compression of pre-aged specimens can lower low-frequency dielectric loss through partial closure of existing cracks, even though the insulation has already deteriorated. A lower loss value alone therefore cannot establish recovery or exclude damage. Temperature and moisture conditions should be recorded when comparing dielectric responses, and changes in discharge activity or winding response should be checked against the thermal and structural observations. Agreement among several indicators provides a stronger basis for inspection or maintenance decisions than a single diagnostic quantity.

The present experiments establish relationships for PET films subjected to sustained compression, including specimens with prior thermal or damp-heat exposure. In an operating reactor, these stresses can occur simultaneously, and electrical discharges can further modify the damage. The proposed measures and assessment approach are engineering implications of the results; their effectiveness and diagnostic thresholds require validation on representative winding structures. Simultaneous multistress tests and comparisons with service-aged insulation are needed before a quantitative condition index or remaining-life model can be established.

5. Conclusions

Through aging experiments and property characterization of polyester film sheet specimens, this study systematically clarified the mechanical deterioration mechanism of inter-turn insulation materials in dry-type air-core reactors under different single-factor stresses and revealed the influence of each stress on material properties. The main conclusions are as follows.

(1) After compressive stress aging of initially unaged specimens, the withstand count decreases significantly with increasing stress and aging time. Low compressive stress only induced a small quantity of microcracks, while high stress accelerated crack initiation and propagation, formed electric field concentration regions, and accelerated electrical breakdown. Mechanical stress has an obvious degradation-promoting effect on thermal- or damp-heat-pretreated specimens. At the same stress level, withstand count is positively correlated with mechanical strength. Because damp-heat aging causes early molecular-chain scission and severe mechanical-property degradation, cracks in these specimens are more likely to interconnect under compressive stress, resulting in the most pronounced decline in insulation performance.

(2) After mechanical stress aging, dielectric loss increases over the entire frequency range, with a more pronounced increase at the initial stage. This indicates that stress not only generates microcracks and increases interfacial-polarization loss, but also reduces insulation resistance and increases conductive loss. The loss of thermal- and damp-heat-aged specimens increases monotonically, with a larger increase observed for damp-heat aged specimens. When stress is applied to already degraded specimens, the low-frequency dielectric loss first decreases and then increases, which is associated with the size and number of microcracks and the strength of interfacial polarization.

Author Contributions: Conceptualization, H.N.; Methodology and experimental design, M.X.; Resources, C.L.; Visualization, X.W. and Z.W.; Writing—original draft and manuscript integration, F.C. All authors have read and agreed to the published version of the manuscript.

Funding: This research was funded by the Science and Technology Project of State Grid Heilongjiang Electric Power Company Limited, entitled 'Research on Inter-Turn Insulation Detection and Monitoring Mechanisms and Device Development for Dry-Type Air-Core Reactors' (grant number 522437250007).

Data Availability Statement: The data presented in this study are included in the article.

Conflicts of Interest: Authors Minhu Xu, Chang Liu, Xuedong Wang, and Zhenchuan Wang were employed by Heilongjiang Electric Power Research Institute. The remaining authors declare that the research was conducted in the absence of any commercial or financial relationships that could be construed as a potential conflict of interest. The authors declare that this study received funding from State Grid Corporation of China through its Science and Technology Project (grant number 522437250007). The funder was involved in the study through its affiliated co-authors, whose contributions included experimental design, specimen preparation, and visualization, as detailed in the Author Contributions section.

References

1. Kroposki, B.; Johnson, B.; Zhang, Y.; Gevorgian, V.; Denholm, P.; Hodge, B.-M.; Hannegan, B. Achieving a 100% renewable grid: Operating electric power systems with extremely high levels of variable renewable energy. *IEEE Power Energy Mag*. **2017**, *15*, 61–73. [CrossRef]
2. Mohammed, A.; Sakr, E.K.; Abo-Adma, M.; Elazab, R. A comprehensive review of advancements and challenges in reactive power planning for microgrids. *Energy Inform*. **2024**, *7*, 63. [CrossRef]
3. Enohnyaket, M.; Ekman, J. Analysis of air-core reactors from DC to very high frequencies using PEEC models. *IEEE Trans. Power Deliv*. **2009**, *24*, 719–729. [CrossRef]
4. Avilla-Montes, J.; Apodaca, E.; Melgoza, E.; Cardenas, A. Analysis of a virtual-gap reactor as a shunt compensation device. In Proceedings of the 2016 IEEE International Autumn Meeting on Power, Electronics and Computing (ROPEC), Ixtapa, Mexico, 9–11 November 2016.
5. Ma, Z.; Wang, G.; Jiang, D.; Yang, X.; Shu, X. Design and application of non-contact voltage acquisition module for dry air core reactor. In *Frontier Academic Forum of Electrical Engineering*; Springer: Singapore, 2022; pp. 173–183.
6. Jin, S.; Zhu, L.; Li, C.; Yang, Y.; Wu, Z. Research on the diagnosis method of inter-turn short-circuit faults of dry-type air-core reactor winding based on frequency response analysis. *AIP Adv*. **2024**, *14*, 065015. [CrossRef]
7. Zhang, H.; Zhang, W.; Jiao, B. Analysis of inter-turn short circuit characteristics in the windings of dry-type air-core series and shunt reactors. In Proceedings of the 2024 IEEE 7th International Conference on Automation, Electronics and Electrical Engineering (AUTEEE), Shenyang, China, 27–29 December 2024.
8. Wu, J.; Zhen, W.; Chang, Z. A detection method for slight inter-turn short-circuit fault in dry-type air-core shunt reactors. *Energies* **2024**, *17*, 1709. [CrossRef]
9. Kavanagh, D.F.; Gyftakis, K.N.; McCulloch, M.D. Thermal degradation phenomena of polymer film on magnet wire for electromagnetic coils. *IEEE Trans. Ind. Appl*. **2020**, *57*, 458–467. [CrossRef]
10. Zhang, J.; Li, Z.; Liu, H.; Liang, J.; Yang, H.; Zhang, P. Study on the aging characteristics of reactor encapsulating insulation based on time-domain dielectric response. In Proceedings of the International Conference on Information Optics and Optoelectronics Technology (CIOT 2024), Dali, China, 22–24 November 2024.
11. Nie, H.; Li, Z.; Mei, Z.; Wang, Y.; Yao, Y. Influence of dry-type air-core reactor turn-to-turn overvoltage waveform parameters on the deterioration law of insulating materials. *IEEE Access* **2025**, *13*, 176410–176420. [CrossRef]
12. Wei, X.; Yu, C.; Liang, J.; Liu, H. Effect of thermal aging on interturn insulation properties of dry-type air-core power reactors. In Proceedings of the 2020 5th Asia Conference on Power and Electrical Engineering (ACPEE), Chengdu, China, 4–7 June 2020.
13. Kawada, H.; Goto, K.; Hanamura, M.; Suzuki, K. Switching surge of shunt reactor caused by SF6 circuit breaker operation. *IEEE Trans. Power Deliv*. **1987**, *2*, 1124–1130. [CrossRef]
14. Akin, F.; Arikan, O. The effect of thermal aging on solid insulating materials: A case study for dielectric loss and dissipation factor based evaluations under different voltage levels and frequencies. *Eng. Fail. Anal*. **2023**, *148*, 107222. [CrossRef]
15. Lu, Z.; Zeng, L.; Liu, Y.; Wang, X. Simulation analysis of inter-turn short-circuit fault of dry-type air-core reactor. In Proceedings of the 2023 IEEE 6th International Conference on Automation, Electronics and Electrical Engineering (AUTEEE), Shenyang, China, 15–17 December 2023.
16. Nie, H.; Wei, X.; Yao, Y.; Mei, Z.; Wang, Y. Influence of thermal aging on switching-overvoltage withstand characteristics of inter-turn insulation in dry-type air-core power reactors. *Trans. China Electrotech. Soc*. **2020**, *35*, 5096–5104.
17. Nie, H.; Zhang, C.; Gu, Z.; Yao, Y.; Liu, X. The research on electrical aging characteristics of turn-to-turn insulation of dry-type air core reactor under partial discharge. *Trans. China Electrotech. Soc*. **2018**, *33*, 3071–3079.

18. Yuan, Z.; Wang, Q.; Ren, Z. Investigating aging characteristics of oil-immersed power transformers' insulation in electrical–thermal–mechanical combined conditions. *Polymers* **2023**, *15*, 4239. [CrossRef] [PubMed]
19. Lin, H.; Guo, J.; Huang, X. Insight on atmospheric hydrothermal aging for polyester and polyimide film used in dry-type reactor. *Coatings* **2023**, *13*, 253. [CrossRef]
20. Liu, L.; Wang, Y.; Francisco, C.; Andrade, R. Atmospheric corrosion-induced interturn short circuit in a 21 kV dry-type air-core shunt reactor. In Proceedings of the 2026 11th Asia Conference on Power and Electrical Engineering (ACPEE), Macao, China, 14–17 April 2026; pp. 1282–1288.
21. Xu, K.; Ao, M.; Zhao, C.; Li, Z. Simulation of microcrack strain and stress of encapsulated insulation in reactor with air core. *Transformer* **2016**, *53*, 34–37.
22. Bian, B.; Xia, G.; Li, J. Thermal-aging characteristics of epoxy/glass fiber composite materials for dry-type air-core reactors. *Polym. Compos.* **2021**, *42*, 3773–3785. [CrossRef]
23. *GB/T 10229-1988*; Reactors. TC44: Shenyang, China, 1988; National Public Service Platform for Standards Information. Available online: https://std.samr.gov.cn/gb/search/gbDetailed?id=71F772D75FF7D3A7E05397BE0A0AB82A (accessed on 28 October 2026). (In Chinese)
24. *IEC 60289:1988*; Reactors. 2nd ed. International Electrotechnical Commission: Geneva, Switzerland, 1988.
25. Hui, B.; Peng, Y.; Fu, M.; Xu, M.; Hou, S. Breakdown characteristics of silicone rubber under mechanical stress. *Insul. Mater.* **2019**, *52*, 29–35.
26. Chen, L.; Wang, J.; Liu, R.; Liu, C.; Xiang, T. Insulation detection system of dry-type air-core reactor based on oscillation wave. *J. Shenyang Univ. Technol.* **2020**, *42*, 601–606. [CrossRef]

Disclaimer/Publisher's Note: The statements, opinions and data contained in all publications are solely those of the individual author(s) and contributor(s) and not of MDPI and/or the editor(s). MDPI and/or the editor(s) disclaim responsibility for any injury to people or property resulting from any ideas, methods, instructions or products referred to in the content.